Wear 306 (2013) 27–35

Contents lists available at ScienceDirect

Wear

journal homepage: www.elsevier.com/locate/wear

Corrosion and tribocorrosion behaviour of Al–Si–Cu–Mg alloy and its composites reinforced with B_4C particles in 0.05 M NaCl solution

F. Toptan [a,b,*], A.C. Alves [b], I. Kerti [a], E. Ariza [b,c], L.A. Rocha [b,d]

[a] Yildiz Technical University, Department of Metallurgical and Materials Engineering, Faculty of Chemistry & Metallurgy, Davutpasa Campus, 34210 Esenler, Istanbul, Turkey
[b] Centre for Mechanics and Materials Technologies (CT2M), Universidade do Minho, Azurém, 4800-058 Guimarães, Portugal
[c] Universidade do Minho, SEMAT/UM, Azurém, 4800-058 Guimarães, Portugal
[d] UNESP—Univ. Estadual Paulista, Faculdade de Ciências de Bauru, Dep. Física, 17033-360 Bauru, SP, Brazil

ARTICLE INFO

Article history:
Received 22 November 2012
Received in revised form
17 June 2013
Accepted 26 June 2013
Available online 6 July 2013

Keywords:
Metal–matrix composite
Corrosion–wear
Wear testing

ABSTRACT

The corrosion behaviour of metal matrix composites (MMCs) is strictly linked with the presence of heterogeneities such as reinforcement phase, microcrevices, porosity, secondary phase precipitates, and interaction products. Most of the literature related to corrosion behaviour of aluminium matrix composites (AMCs) is focused on SiC reinforced AMCs. On the other hand, there is very limited information available in the literature related to the tribocorrosion behaviour of AMCs. Therefore, the present work aims to investigate corrosion and tribocorrosion behaviour of Al–Si–Cu–Mg alloy matrix composites reinforced with B_4C particulates. Corrosion behaviour of 15 and 19% (vol) B_4C reinforced Al–Si–Cu–Mg matrix composites and the base alloy was investigated in 0.05 M NaCl solution by performing immersion tests and potentiodynamic polarisation tests. Tribocorrosion behaviour of Al–Si–Cu–Mg alloy and its composites were also investigated in 0.05 M NaCl solution. The tests were carried out against alumina ball using a reciprocating ball-on-plate tribometer. Electrochemical measurements were performed before, during, and after the sliding tests together with the recording of the tangential force. Results suggest that particle addition did not affect significantly the tendency of corrosion of Al–Si–Cu–Mg alloy without mechanical interactions. During the tribocorrosion tests, the counter material was found to slide mainly on the B_4C particles, which protected the matrix alloy from severe wear damage. Furthermore, the wear debris were accumulated on the worn surfaces and entrapped between the reinforcing particles. Therefore, the tendency of corrosion and the corrosion rate decreased in Al–Si–Cu–Mg matrix B_4C reinforced composites during the sliding in 0.05 M NaCl solution.

© 2013 Elsevier B.V. All rights reserved.

1. Introduction

Aluminium is one of the most reactive metals with high affinity to oxygen. However, due to the inert and protective characteristics of the aluminium oxide film that forms on the metal surface, Al is highly resistant to most atmospheres as well as a great variety of chemical agents [1].

Al–Si casting alloys are widely used in the automotive industry, mainly due to their high castability and high mechanical properties. Both the hypo-eutectic and hyper-eutectic Al–Si alloys are being used for several tribological applications, such as internal combustion engines, pistons, liners, clutches, pulleys, rockers and pivots [2,3]. Mechanical strength of these alloys can be improved by the addition of copper, where precipitation hardening leads to the controlled precipitation of Cu-rich precipitates (usually metastable intermetallic Al_2Cu phases) that form obstacles for dislocation movements [3,4]. However, due to the noble behaviour of this phase, existence of the galvanic coupling with the surrounding matrix may lead to several consequences on the corrosion resistance. It is well known that the Al_2Cu phase acts as a preferential cathode for the oxygen reduction reaction and therefore accelerates the oxidation of aluminium. Furthermore, the OH^- produced during oxygen reduction can locally increase the pH, and may lead to the local dissolution of the Al-matrix in the surroundings of the preferential cathodes [3,5].

In MMCs, the composition of the matrix material, the reinforcement phase, microcracks, residual stresses, microcrevices, porosity, secondary phase precipitates, and interaction products may significantly affect the corrosion behaviour [6–9]. The main causes of the corrosion in MMCs are reported as (i) galvanic coupling between the matrix and the reinforcement materials, (ii) selective

* Corresponding author at: Centre for Mechanics and Materials Technologies (CT2M), Universidade do Minho, Azurém, 4800-058 Guimarães, Portugal.
Tel.: +351 253 510 220; fax: +351 253 516 007.
E-mail address: ftoptan@dem.uminho.pt (F. Toptan).

0043-1648/$ - see front matter © 2013 Elsevier B.V. All rights reserved.
http://dx.doi.org/10.1016/j.wear.2013.06.026

Table 1
Chemical composition of Al–Si–Cu–Mg matrix material.

Al	Si	Fe	Mn	Cr	Ni	Cu	Mg	Pb	Sn	Ti	Zn
82.8	10.14	1.29	0.432	0.021	0. 032	2.99	1.49	0.372	0.008	0.084	0.616

corrosion at the matrix/reinforcement interface, (iii) chemical degradation of interphases and reinforcement materials, and (iv) corrosion of matrix defects [10,11].

Most of the literature related to corrosion behaviour of AMCs is focused on SiC reinforced AMCs, and pitting is reported as the most common corrosion type in these composites [12]. On the other hand, there is very limited information available on the corrosion behaviour of Al–B_4C composites. In a recent work, Katkar et al. investigated the corrosion behaviour of AA6061-B_4C (0, 10, 15, and 20% in wt) composites in seawater. The authors stated that corrosion tendency of AA6061-B_4C composites was lower than the unreinforced alloy within the studied conditions, and furthermore, corrosion tendency is decreased with the increasing amount of B_4C particles. However, with increasing amount of B_4C particles, the composites exhibited lower resistance to pitting corrosion [12].

It has been reported that 10% of the material degradation in engineering parts occurs due to corrosion, while 30% is due to abrasion, 15% is due to adhesion, and 10% is due to tribocorrosion [13]. However, even though the tribological characteristics of AMCs have been extensively studied [14,15], there is very limited information available in the literature related to the tribocorrosion behaviour of AMCs. Tribocorrosion has been defined by Landolt et al. as an irreversible transformation of a material resulting from simultaneous physico-chemical and mechanical interactions that occur in a tribological contact [16]. In tribocorrosion systems, the total degradation rate can be different than the sum of the corrosion rate and the wear rate that measured individually [17].

Fang et al. studied the synergistic effects of wear and corrosion for 0–20% (vol) Al_2O_3 particulate reinforced 6061 AMCs, against Al_2O_3 in 3.5% (wt) NaCl solution using a revised block-on-ring wear tester. The authors stated that incorporation of the reinforcement was detrimental to the corrosion resistance of aluminium, however, particle addition improved the tribocorrosion behaviour of the matrix material [18]. Velhinho et al. investigated the tribocorrosion behaviour of Al–SiC_p functionally graded metal matrix composites (FGMMCs) against cast iron pins in water, using a unidirectional pin-on-disc tribometer. Two volume fractions (12.6 and 35.7%) of SiC particles were studied. The authors reported that the presence of water facilitated catastrophic SiC particle pull-out, and therefore increased the material loss significantly. Furthermore, an increase in reinforcing particles content resulted in a poorer wear performance [19]. Gomes et al. also studied tribocorrosion behaviour of Al–SiC_p FGMMCs with volume fractions varying between 25.8 and 33.4%. Experiments performed against cast iron pins in 3% NaCl solution using reciprocating sliding. The authors reported that the wear rate of the composites was not significantly affected by the presence of the aqueous solution [20]. Besides, as opposed to Velhinho et al. [19], higher amounts of reinforcement lead to lower wear rates, indicating that the presence of NaCl can have some influence on the tribocorrosion mechanisms. The authors attributed this behaviour to the ability of higher amount of reinforcing particles to anchor iron-rich protective tribolayers and load-supporting effect given by SiC particles. Vieira et al. studied the tribocorrosion behaviour of Al–SiC_p FGMMCs against alumina ball in 0.05 M NaCl solution using a ball-on-plate tribometer. After triboelectrochemical studies on 11–23% (vol) composites, the authors stated that the introduction of SiC particles did not affect the corrosion behaviour of the composites. The authors reported two tribocorrosion mechanisms depending on the SiC_p content: above 18%, wear accelerated corrosion by protecting effect of protruded SiC particles, and below 18%, wear-accelerated corrosion without any affect of the particles on wear [21]. Ferreira et al. studied tribocorrosion behaviour of Al–Al_3Ti and Al–Al_3Zr FGMMCs against alumina ball in 0.6 M NaCl solution using a reciprocating tribometer. After tribocorrosion studies of up to 17.3% (vol) composites, the authors reported a better tribocorrosion behaviour in the samples having higher volume fraction of particles [22]. Jamaati et al. investigated tribocorrosion behaviour of Al–Al_2O_3 composites against alumina ball in 1 wt% NaCl solution, using a ball-on-plate tribometer. After studying of 0.48–3.55% (vol) reinforced composites, the authors reported that homogenous particle distribution improved the wear and corrosion resistance [23].

There are several studies related to the dry sliding wear behaviour of Al–B_4C composites. However, to the best of our knowledge, there is no information available in the literature related to the tribocorrosion behaviour of these composites. It is worth to emphasize that in many cases, the industrial components (e.g. automotive applications) are required to be operated in aqueous environments (i.e. corrosive media) [24]. Since Al–B_4C composites have been considered as a wear resistant material [25–27], tribocorrosion behaviour of these composites is also needed to be studied, especially before considering them as an alternative material for the applications that are being exposed to a tribocorrosion environment during their lifetime. Thus, the present study aims to investigate the corrosion and tribocorrosion behaviour of 15 and 19% (vol) B_4C reinforced Al–Si–Cu–Mg matrix composites in comparison with its base alloy in 0.05 M NaCl solution.

2. Experimental procedure

2.1. Materials

B_4C particles with an average particle size 32 μm were used as a reinforcement, and Al–Si–Cu–Mg aluminium alloy was used as a matrix material (Table 1). In order to promote the wettability of boron carbide powders and improve their incorporation behaviour into aluminium melts, Al–Si–Cu–Mg matrix B_4C reinforced composites were produced by the addition of K_2TiF_6 flux. The processing procedure and the physical properties of Al–Si–Cu–Mg—B_4C composites having two different volume fractions of 15 and 19% (nominal values of 16 and 22, respectively) are explained elsewhere [28].

2.2. Corrosion tests

Two different corrosion tests were carried out: immersion tests and potentiodynamic polarisation tests. Prior to each test, the samples were grinded and polished using diamond grinders and water based diamond and colloidal silica suspensions down to 0.04 μm. An amount of 0.05 M NaCl (Panreac) used as the electrolyte, saturated calomel electrode (SCE) used as the reference electrode, Pt electrode used as the counter electrode, and samples used as the working electrode in both corrosion tests.

The samples were immersed to the solution for 192 h (8 days). Open circuit potential (OCP) was measured just after immersion during 30 min and after that, for 10 min during the following

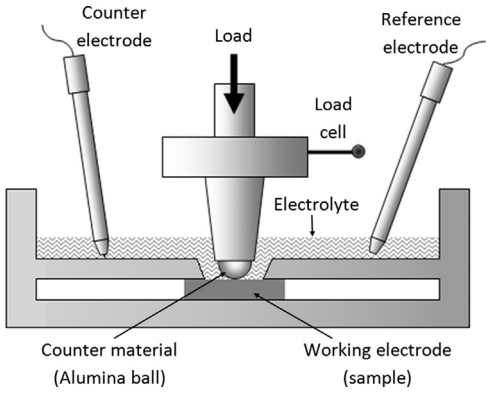


Fig. 1. Schematic view of the tribocorrosion test setup.

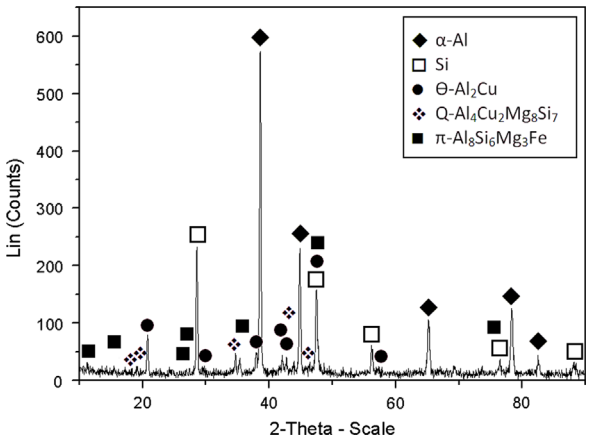


Fig. 2. XRD spectrum of as-cast Al–Si–Cu–Mg alloy.

6 days. The OCP measurements were performed using a Voltalab PGZ 100 potentiostat (Radiometer Analytical, Copenhagen, Denmark) controlled by the VoltaMaster 4 software (Radiometer Analytical, Copenhagen, Denmark).

Polarisation curves were obtained using a Voltalab PGP201 potentiostat (Rodiometer Analytical, Copenhagen, Denmark) controlled by the VoltaMaster 4 software (Radiometer Analytical, Copenhagen, Denmark). Potentiodynamic polarisation measurements started from a cathodic potential of −0.8 V up to the anodic domain (O V vs. SCE) with a scan rate of 0.5 mV/s.

2.3. Tribocorrosion tests

Prior to each test, specimens were prepared following the same procedure for the corrosion tests. Before starting the tests, specimens were cleaned with propanol in ultrasonic cleaner for 10 min and kept in desicator for 1 h.

For the tribocorrosion experiments, the samples were mounted in a cell containing the electrolyte (0.05 M NaCl) and electrodes (Fig. 1). The cell was installed on a ball-on-plate tribometer (CETR-UMT-2) with a reciprocating plate adapter with the working surface area of the samples facing upwards. Alumina ball (10 mm of diameter, Goodfellow) was used as a counter material and it was mounted vertically above the exposed sample area (2.3 cm^2). The ball was loaded and the sliding started in a reciprocating system with total stroke length of 5 mm, frequency of 1 Hz, normal force of 3 N, and total sliding time of 600 s. The electrochemical measurements (OCP and current) were performed using the same three-electrode set-up that used in corrosion tests. OCP and current were measured before, during, and after sliding. For the tribocorrosion tests under potentiostatic conditions, the samples were stabilized in electrolyte and the E_{OCP} values were applied as the potential for each test. All the electrochemical measurements were performed using a Voltalab PGP201 potentiostat (Rodiometer Analytical, Copenhagen, Denmark) controlled by the VoltaMaster 4 software (Radiometer Analytical, Copenhagen, Denmark). The tests were performed at the room temperature (25 ± 1 °C).

2.4. Characterisation

Metallographic samples sectioned from the cast bars were prepared using diamond grinders and water based diamond and colloidal silica suspensions down to 0.04 μm grain size. The microstructure of the as-cast alloy was characterised by XRD (Cu *K*α radiation, Bruker D8 Discover). As-cast microstructures were examined under Leica DM2500 optical microscope (OM) and FEI Nova 200 field emission gun scanning electron microscope (FEG-SEM) equipped with EDAX, energy dispersive X-ray spectroscopy (EDS). Corroded surfaces after immersion, and worn surfaces after tribocorrosion tests were also characterised using FEG-SEM/EDS.

3. Results and discussion

3.1. Material microstructures

As can be observed in the XRD spectrum presented in Fig. 2, the following phases were identified for as-cast Al–Si–Cu–Mg alloy: α-Al, Si, θ-Al_2Cu, Q-$Al_4Cu_2Mg_8Si_7$ and π-$Al_8Si_6Mg_3Fe$. Similar phases were also reported by Vieira et al. [3] for a similar alloy (Al–10Si–4.5Cu–2Mg).

Fig. 3a shows the morphology of each phase as observed by SEM. It is known that ceramic particle addition can change the solidification sequence of MMCs from that of its base alloy. As a result, matrix microsegregation is reduced, crystal morphology is modified from cellular–dendritic (Fig. 3b) to a featureless structure, silicon phase nucleated heterogeneously on particles, and matrix grains are refined (Fig. 3c and d) [29,30]. The modification of the matrix alloy structure may influence the mechanical properties and wear resistance of the composites [31].

3.2. Corrosion tests

3.2.1. Evolution of the open circuit potential with time

Evolution of the open circuit potential (OCP) values of the base Al–Si–Cu–Mg alloy and its composites with time is given in Fig. 4a. As can be seen on the graph, particle addition did not significantly affect the tendency of corrosion of Al–Si–Cu–Mg alloy along time.

It has been reported that in aluminium alloys, noble phases like Al_2Cu, Mg_2Si and Al_3Fe can cause localized corrosion due to the galvanic coupling [3,32]. Fig. 4b shows the representative SEM micrographs taken from the base Al–Si–Cu–Mg alloy after 26 h of immersion. The preferential dissolution around the θ-Al_2Cu phase can be clearly seen on Fig. 4b. However, other phases in the Al–Si–Cu–Mg alloy did not lead to preferential dissolution or galvanic coupling effect. The role of Al_2Cu intermetallic compound in selective corrosion of Al alloys is well studied [5]. The results are in agreement with Vieira et al. where preferential dissolution in the vicinity of θ-Al_2Cu phase was reported for a similar Al–Si–Cu–Mg alloy in the same electrolyte (0.05 M NaCl), whereas no preferential dissolution was reported for any other phase in the alloy [3].

It is known that it is difficult to produce Al–B_4C composites especially at processing temperatures below 1100 °C, due to the poor wetting between Al and B_4C [33–35]. However, by the addition of Ti, it is possible to produce Al–B_4C composites at relatively lower temperatures with higher particle volume

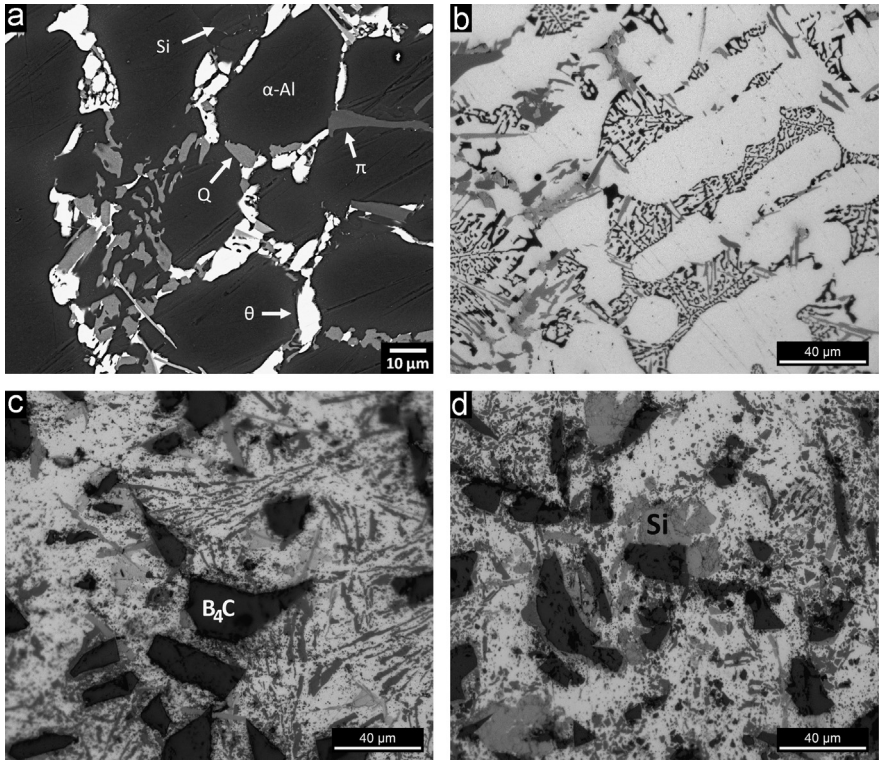


Fig. 3. (a) BSE SEM image and (b) OM image of as-cast Al–Si–Cu–Mg alloy, and OM images of (c) 15% and (d) 19% B_4C reinforced composites.

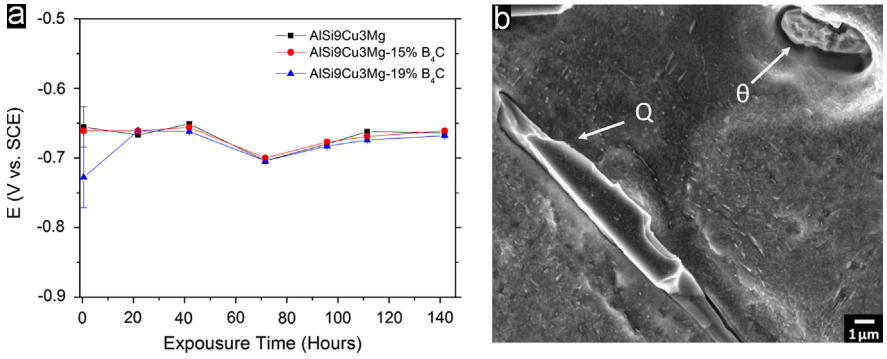


Fig. 4. (a) Evolution of OCP values with time and (b) SE SEM image of *Q* and *θ* phases.

fractions, via formation of TiB_2–TiC reaction layer at the matrix/reinforcement interface. The characterization of the TiB_2–TiC reaction layers at the matrix/reinforcement interfaces for Al–Si–Cu–Mg, AlSi9Mg, AA1070, and AA6063 matrix B_4C reinforced composites have already been reported [28,36–38]. The interfaces play an important role on MMCs and one of the most common corrosion problems in AMCs is the selective corrosion at the matrix/reinforcement interface [10]. It is known that excessive formation of large aluminium carbides at the matrix/reinforcement interface is detrimental to the corrosion resistance of AMCs [39]. The interphases reported for Al–B_4C system are AlB_2, Al_3BC, Al_4BC, $AlB_{24}C_4$, $Al_3B_{48}C_2$ and Al_4C_3. It has been reported that the formation of Al_4C_3 phase can be prevented at the processing temperatures below 1000 °C [40–42]. Furthermore, the reaction layer that contains TiC and TiB_2 forms on the B_4C particles with the addition of Ti acts as a 'reaction barrier' and limits the formation of undesirable interphases that can be formed at the interface [43]. Al_4C_3 formation was not detected on the microstructural studies for the present work. Besides, preferential dissolution was also not observed at the matrix/reinforcement interface responsible for the reaction layer. The EDS analysis taken from the interface

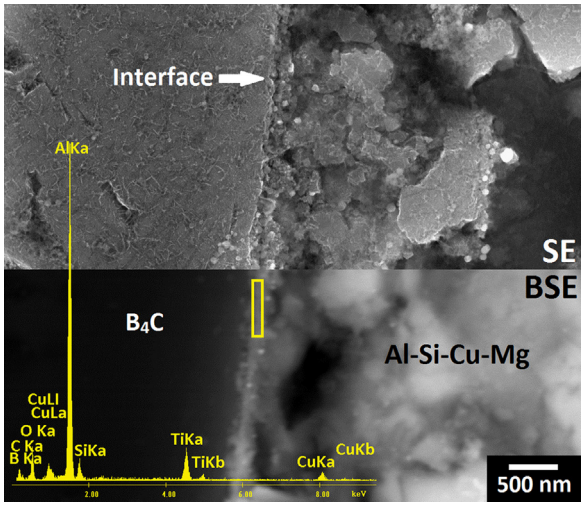


Fig. 5. SE and BSE SEM images from the matrix/reinforcement interface of 15% reinforced composite after 26 h of immersion together with the EDS spectrum taken from the marked area (interface).

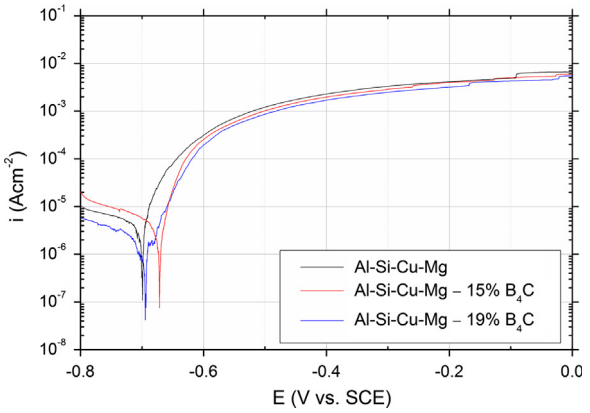


Fig. 6. Polarisation curves of the base Al–Si–Cu–Mg alloy and its composites in 0.05 M NaCl solution.

confirmed that the reaction layer stayed intact at the interface after the immersion (Fig. 5).

3.2.2. Potentiodynamic polarisation tests

Polarisation curves of the base Al–Si–Cu–Mg alloy and the composite samples in 0.05 M NaCl solution are given in Fig. 6. Passive plateau was not observed on the polarisation curves probably due to the preferential dissolution around the θ-Al_2Cu phase. Corrosion potential and current density values were also calculated by Tafel extrapolation method (Table 2). It can be seen from the table that the corrosion current density (i_{corr}) values were decreased by B_4C particle addition. It has been reported that addition of inert particles into a metal can increase the corrosion resistance of the metal by the inert physical barrier role of the particles [44,45]. Thus, the decrease on the i_{corr} values may be due to the effect of the B_4C particles. However, it has also been reported that incorporation of inert material may also shift the corrosion potential ($E_{(i=0)}$) to more noble values by diminishing the exposed metallic area [46,47]. However, a clear correlation between particle volume fraction and corrosion potential has not been observed in the present study. Trzaskoma and Mccafferty studied the effect of SiC reinforcement on the corrosion behaviour of SiC/Al MMCs in 0.1 and 0.6 N NaCl solution and reported that the polarization behaviour of the alloys and composites were similar, and the effect of SiC reinforcements on the corrosion potential was not clear. The authors also stated that the addition of SiC may result more positive, more negative, or unchanged corrosion potential values depending on the alloy system and deaeration conditions [48]. But besides, anodic and cathodic polarisation of the unreinforced alloy and the composites presented similar character (Fig. 6). Katkar et al. investigated the influence of B_4C addition (10, 15, and 20% in wt) to the polarisation behaviour of AA6061 alloy and reported the minimum corrosion current density (i_{corr}) for the unreinforced alloy. Furthermore, the authors also reported that the character of anodic and cathodic polarisation curves for B_4C reinforced composites were very similar to that of its unreinforced alloy [12]. Vieira et al. studied the polarisation behaviour of Al–10Si–4.5Cu–2Mg matrix SiC reinforced FGMs and obtained similar behaviour for the unreinforced alloy and the SiC reinforced FGMs. Furthermore, the authors reported similar $E_{(i=0)}$ values both for the unreinforced alloy and the FGMs (~ -0.60 V vs SCE) [21].

3.3. Tribocorrosion

3.3.1. Electrochemical measurements

The evolution of the OCP and the current density with time before, during, and after the sliding are given in Fig. 7 for the unreinforced alloy and the composites, together with the COF

Table 2
Corrosion potential ($E_{(i=0)}$)and corrosion current density (i_{corr}) values.

Sample	$E_{(i=0)}$ (mV)	i_{corr} (μA/cm^2)
Al–Si–Cu–Mg	-696.5 ± 4	4.22 ± 0.35
Al–Si–Cu–Mg–15% B_4C	-655.8 ± 15	4.03 ± 0.54
Al–Si–Cu–Mg–19% B_4C	-694.0 ± 2	2.64 ± 0.16

values obtained during the sliding (COF values presented very similar evolution in both electrochemical tests). In the unreinforced alloy, when sliding started, OCP values started to decrease and current density values started to increase, and after a certain point, the values stayed relatively stable till the end of the sliding. This is a well known behaviour for the passive metals; when sliding starts, due to the periodically removing of the passive film caused by the mechanical action following by exposure of fresh active material that becomes contact with the solution, tendency to corrosion and corrosion rate increase [21,22,49]. However, an opposite behaviour was observed for the composites for both OCP and current density curves. When sliding started, instead of decreasing, OCP values slightly increased. After sliding, the OCP values recovered and became stable near the values recorded before the sliding started, even though the recovering time was shorter (approx. 2 min) compared to the base Al–Si–Cu–Mg alloy (approx. 3 min). On the other hand, sudden drops were recorded on the current density values of the composites in the very beginning of the sliding. After that, the evolution was generally below the initial values during the sliding with a relatively stable evolution during the second half of the sliding. After sliding, the values were recovered quickly near the starting values both for the unreinforced alloy and the composites. Similar behaviour of the OCP and current density evolution under sliding was also observed by Gomes et al. and Mathew et al., respectively. It has been reported in the aforementioned study of Gomes et al. that an increase on the OCP values of Al–SiC composites was occurred due to a protective character of the film which formed on the samples' surface by a transfer from the counter material and anchored between the reinforcing particles [20]. Besides, Mathew et al. reported the reduction in the current density during the sliding action due to the accumulation of the wear debris and corrosion products in the contact zone for the tribocorrosion behaviour of the TiC_xO_y thin films in artificial sweat solution [50].

3.3.2. Microstructural analysis of the worn surfaces

In order to understand the tribocorrosion mechanism, microstructures of the worn surfaces were investigated by FEG-SEM. All micrographs are taken as parallel to the sliding direction and the microstructures exhibited similar features after both electrochemical tests.

The width of the wear tracks were microscopically measured as approx. 682, 602, and 347 μm for the unreinforced alloy, and its composites with 15 and 19% B_4C, respectively. It is well known that addition of hard particles increases the wear resistance of the base aluminium alloy [51–55]. Furthermore, it is also known that microstructure modification in Al–Si and Al–Si–Cu alloys leads to improvement on the wear resistance [56–59]. Therefore, even though no study were performed in order to measure the wear loss volume, it may be suggested from the microscope investigations (i.e. width of the wear track) that B_4C particle addition caused a better response to wear on the Al–Si–Cu–Mg alloy matrix composites in 0.05 M NaCl solution, probably mainly due to the load bearing effect of the reinforcing particles, but also might be contributed by the increased wear resistance of the modified matrix alloy.

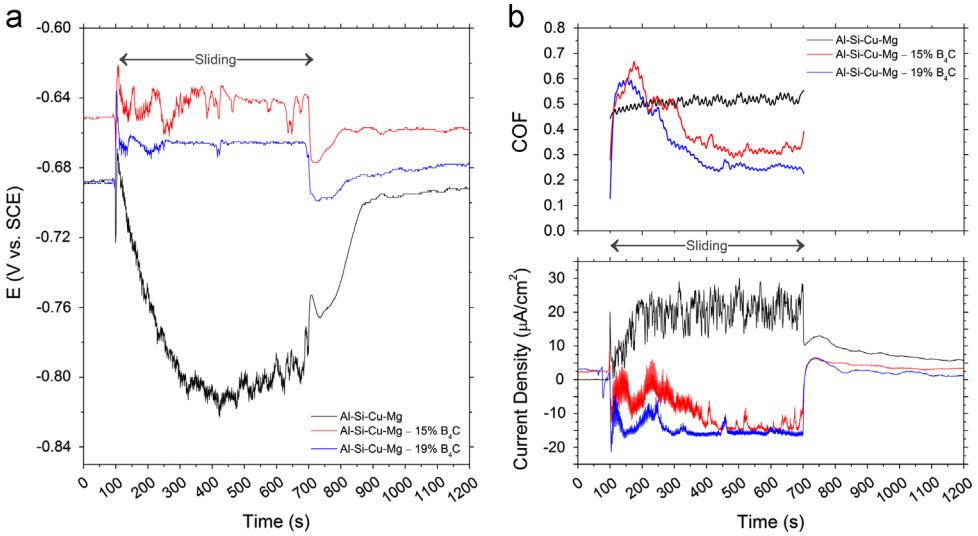


Fig. 7. The evolution of the (a) OCP and (b) current density together with the evolution of the COF values during sliding.

It is observed that the wear tracks were darker than the outer area. Since the images are taken in BSE-mode, this points to a compositional change between the worn and the unworn areas. EDS analyses taken from those two areas showed that oxygen content of worn areas is higher than the unworn areas for each specimen. At higher magnification, the worn surfaces showed following features: (i) grooves, (ii) higher oxide content in the worn area, (iii) cracks on the alloy due to plastic deformation, (iv) particle pull-outs (voids), (v) broken particles, and (vi) smoother particle surfaces in worn area.

In the present work, normal load is chosen as 3 N which results higher initial Hertzian contact pressures (473 MPa) that is higher than the yield strength of the base alloy (approx. 193 MPa [60]). It is considered that this relatively higher contact pressures lead to plastic deformation during the sliding. Fig. 8a shows the cracks on the base Al–Si–Cu–Mg alloy due to plastic deformation. It has been deduced that this relatively higher contact pressure also resulted removing some of the weakly attached particles (Fig. 8b) as well as some particle cracking (Fig. 8c). Even though, it is also observed that most of the particles stayed intact on the surface after sliding (Fig. 8d). On the other hand, when the surfaces of the particles inside the worn area were investigated, it was observed that those surfaces were much smoother (Fig. 8e) than the ones from the unworn area (Fig. 8f). This can be attributed to the load bearing effect of the reinforcing particles. Therefore, it can be suggested that during the sliding, the load is mainly carried by the B_4C particles, and therefore particle surfaces were 'polished' by the counter material. Besides, wear debris were accumulated between the load-carrying particles, and even though the samples were cleaned after the tests, it was still possible to observe the accumulations on the microstructural observations (Fig. 8d).

3.3.3. *Tribocorrosion mechanism*

After triboelectrochemical and microstructural studies, the wear mechanism under tribocorrosion conditions has been suggested as following:

(i) *Unreinforced alloy:* Under mechanical solicitation, during the approx. 3–5 min of the sliding, while the OCP and the current density values were increasing COF values were slightly increased (Fig. 7). It is deduced that with the beginning of the sliding, partially oxidised wear debris started to be accumulated on the surface, and during the sliding those debris were packed on the surface by the counter material. Therefore, both electrochemical values and the COF values presented relatively stable values during the rest of the sliding.

(ii) *Composites:* Both 15 and 19% B_4C reinforced composites presented lower COF values at the very beginning of the sliding (Fig. 7). It is deduced that those lower COF values indicate a ceramic–ceramic contact and therefore, it is suggested that the counter material was mainly in contact with the B_4C particles at the onset of the sliding (Fig. 9a). As sliding continued, when the counter material met a protruded B_4C particle (Fig. 9b), local increments were recorded on the COF values (Fig. 7). If that protruded particle was weakly attached on the matrix, it pulled-out or broke, as shown in the micrographs presented in Fig. 8b and c. On the other hand, if particle pull-out happened, a fresh active metal became contact with the solution (Fig. 9c) which led to decrease in the OCP values and increase in the current density values (Fig. 7). In the second half of sliding, most of the weak protruding particles were removed from the surface and/or broke and therefore, the COF values were more stable around 0.3 indicating the ceramic–ceramic contact. Moreover, since the load was mainly carried by the reinforcing particles, metal surface was mainly not in contact with the counter material. Besides, even though there is no total passivation on the metal due to the preferential dissolution around the θ-Al_2Cu phase, fresh metal surfaces after particle pull-outs partially repassivated, furthermore the wear debris were accumulated on the metal surface and entrapped between the B_4C particles (Fig. 9d). Similar to the systems studied by Gomes et al. [20] and Mathew et al. [50], this wear debris accumulation led to a more protective metal surface, thus higher OCP values and lower current density values were observed as compared to the un-sliding stage.

After this first approach to the tribocorrosion behaviour of the Al–B_4C composites, there is a need of further studies in order to have a deeper understanding on the tribocorrosion behaviour of these composites. First, the accumulated wear debris or tribolayer that is acted as a protective layer should be microstructurally (i.e. cross-sectional microstructural and chemical analysis) and electrochemically (i.e. electrochemical impedance spectroscopy) analysed in order to understand the protective characteristics better. Further, tribocorrosion tests should be performed on various potentials, and individual contributions of wear, corrosion, and their synergistic effects on material degradation should be quantified.

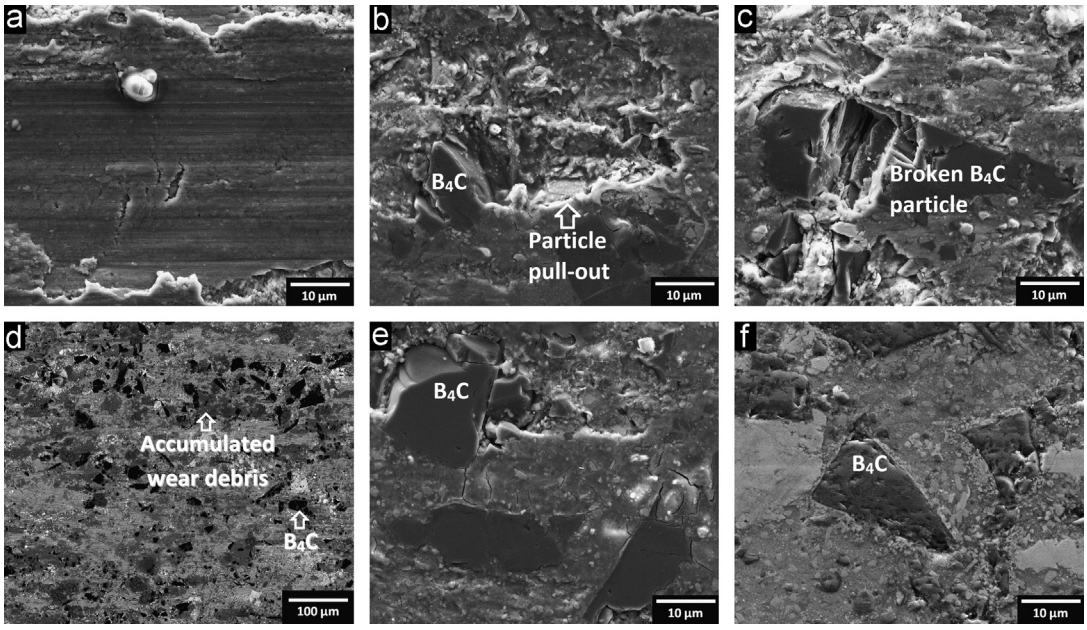


Fig. 8. SEM images after tribocorrosion tests under potentiostatic conditions representing (a) plastic deformation on the Al–Si–Cu–Mg sample (SE), (b) particle pull-out and (c) broken particle on the Al–Si–Cu–Mg—15% B_4C sample (SE), (d) wear track of the Al–Si–Cu–Mg—15% B_4C sample (BSE), (e) load bearing particles on the wear track of the Al–Si–Cu–Mg—15% B_4C sample and (f) particles on the unworn area of the Al–Si–Cu–Mg—19% B_4C sample (SE).

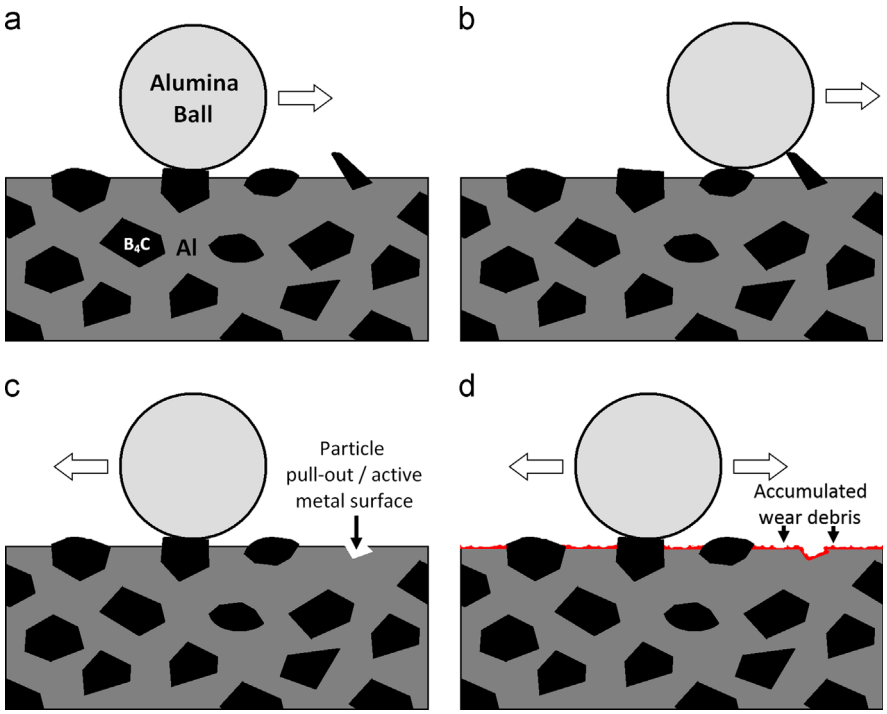


Fig. 9. Schematic view of the suggested tribocorrosion mechanism; (a) in the beginning of the sliding, the counter material is in contact with B_4C particles, (b) the counter material meets with a protruded particle and (c) after particle pull-out, a fresh active metal becomes contact with the solution and finally (d) the surface of the metal is covered by the accumulated wear debris.

4. Conclusions

Corrosion and tribocorrosion behaviour of the base Al–Si–Cu–Mg alloy and its composites reinforced with B_4C particles were investigated in 0.05 M NaCl solution. After electrochemical, tribological and microstructural studies, the followings can be concluded:

(1) Particle addition did not affect significantly the tendency of corrosion of Al–Si–Cu–Mg alloy.

(2) Passive plateau was not observed on the polarisation curves due to the preferential dissolution around the θ-Al_2Cu phase.

(3) After immersion, preferential dissolution was not observed in the vicinity of the reinforcement particles, and the matrix/reinforcement reaction layer stayed intact during the immersion.

(4) During the tribocorrosion tests, the counter material was found to slide mainly on the B_4C particles, which protected the matrix alloy from severe corrosion/wear damage.

Furthermore, the wear debris were accumulated on the worn surface and entrapped between the reinforcing particles. Therefore, the tendency of corrosion and the corrosion rate decreased in Al–Si–Cu–Mg matrix B_4C reinforced composites during the sliding in 0.05 M NaCl solution.

Acknowledgements

This study was partially supported by TUBITAK (The Scientific and Technological Research Council of Turkey) under Project No. 107M338, and Centre for Mechanical and Materials Technologies (CT2M) in Portugal.

References

[1] L. Shreir, third ed.,Corrosion, vol. 1, Butterworth-Heinemann, London, 1994.
[2] H. Ahlatci, E. Candan, H. Çimenoğlu, Abrasive wear behavior and mechanical properties of Al–Si/SiC composites, Wear 257 (2004) 625–632.
[3] A.C. Vieira, A.M. Pinto, L.A. Rocha, S. Mischler, Effect of Al_2Cu precipitates size and mass transport on the polarisation behaviour of age-hardened Al–Si–Cu–Mg alloys in 0.05 M NaCl, Electrochimica Acta 56 (2011) 3821–3828.
[4] E. Sjölander, S. Seifeddine, The heat treatment of Al–Si–Cu–Mg casting alloys, Journal of Materials Processing Technology 210 (2010) 1249–1259.
[5] B. Mazurkiewicz, A. Piotrowski, The electrochemical behaviour of the Al_2Cu intermetallic compound, Corrosion Science 23 (1983) 697–707.
[6] T.M. Yue, Y.X. Wu, H.C. Man, Improvement in the corrosion resistance of aluminum 2009aSiC w composite by Nd/YAG laser surface treatment, Journal of Materials Science Letters 18 (1999) 173–175.
[7] J. Hu, W.Y. Chu, W.D. Fei, L.C. Zhao, Effect of interfacial reaction on corrosion behavior of alumina borate whisker reinforced 6061Al composite, Materials Science and Engineering A 374 (2004) 153–159.
[8] A. Pardo, M.C. Merino, S. Merino, F. Viejo, M. Carboneras, R. Arrabal, Influence of reinforcement proportion and matrix composition on pitting corrosion behaviour of cast aluminium matrix composites (A3xx.x/SiCp), Corrosion Science 47 (2005) 1750–1764.
[9] A. Pardo, M.C. Merino, J. Rams, S. Merino, F. Viejo, M. Campo, Effect of reinforcement coating on the oxidation behavior of AA6061/SiC/20p composite, Oxidation of Metals 63 (2005) 215–227.
[10] S. Winkler, H. Flower, Stress corrosion cracking of cast 7XXX aluminium fibre reinforced composites, Corrosion Science 46 (2004) 903–915.
[11] B. Bobic, S. Mitrovic, M. Babic, I. Bobic, Corrosion of aluminium and zinc–aluminium alloys based metal–matrix composites, Tribology in Industry 31 (2009) 44–53.
[12] V.A. Katkar, G. Gunasekaran, A.G. Rao, P.M. Koli, Effect of the reinforced boron carbide particulate content of AA6061 alloy on formation of the passive film in seawater, Corrosion Science 53 (2011) 2700–2712.
[13] J.-P. Celis, P. Ponthiaux, Testing tribocorrosion of passivating materials supporting research and industrial innovation: handbook, in: J.-P. Celis, P. Ponthiaux (Eds.), Testing Tribocorrosion of Passivating Materials Supporting Research and Industrial Innovation: Handbook, W.S. Maney & Son Ltd., Leeds, 2012, pp. 1–13.
[14] C. Díaz, J.L. González-Carrasco, G. Caruana, M. Lieblich, Ni_3Al intermetallic particles as wear-resistant reinforcement for Al-base composites processed by powder metallurgy, Metallurgical and Materials Transactions A: Physical Metallurgy and Materials Science 27A (1996) 3259–3266.
[15] K.M. Shorowordi, A.S.M.A. Haseeb, J.P. Celis, Tribo-surface characteristics of Al–B_4C and Al–SiC composites worn under different contact pressures, Wear 261 (2006) 634–641.
[16] D. Landolt, S. Mischler, M. Stemp, Electrochemical methods in tribocorrosion: a critical appraisal, Electrochimica Acta 46 (2001) 3913–3929.
[17] P. Jemmely, S. Mischler, D. Landolt, Tribocorrosion behaviour of Fe–17Cr stainless steel in acid and alkaline solutions, Tribology International 32 (1999) 295–303.
[18] C. Fang, C.C. Huang, T.H. Chuang, Effects of wear and corrosion for Al_2O_3 particulate–reinforced 6061 aluminum matrix composites, Metallurgical and Materials Transactions A: Physical Metallurgy and Materials Science 30A (1999) 643–651.
[19] A. Velhinho, J.D. Botas, E. Ariza, J.R. Gomes, L.A. Rocha, Tribocorrosion studies in centrifugally cast Al-matrix SiC p-reinforced functionally graded composites, Materials Science Forum 455–456 (2004) 871–875.
[20] J.R. Gomes, A.R. Ribeiro, A.C. Vieira, A.S. Miranda, L.A. Rocha, Wear mechanisms in functionally graded aluminium matrix composites? Effect of the lubrication by an aqueous solution, Materials Science Forum 493 (2005) 33–38.
[21] A.C. Vieira, L.A. Rocha, S. Mischler, Influence of SiC reinforcement particles on the tribocorrosion behaviour of Al–SiC p FGMs in 0.05 M NaCl solution, Journal of Physics D: Applied Physics 44 (2011) 185301.
[22] S.C. Ferreira, P.D. Sequeira, Y. Watanabe, E. Ariza, L.A. Rocha, Microstructural characterization and tribocorrosion behaviour of Al/Al_3Ti and Al/Al_3Zr FGMs, Wear 270 (2011) 806–814.
[23] R. Jamaati, M.R. Toroghinejad, J.A. Szpunar, D. Li, Tribocorrosion behavior of aluminum/alumina composite manufactured by anodizing and ARB processes, Journal of Materials Engineering and Performance 20 (2011) 1600–1605.
[24] F. Bratu, L. Benea, J.-P. Celis, Tribocorrosion behaviour of Ni–SiC composite coatings under lubricated conditions, Surface and Coatings Technology 201 (2007) 6940–6946.
[25] F. Bedir, Characteristic properties of Al–Cu–SiC_p and Al–Cu–B_4C_p composites produced by hot pressing method under nitrogen atmosphere, Materials & Design 28 (2007) 1238–1244.
[26] J. Jung, S. Kang, Advances in manufacturing boron carbide–aluminum composites, Journal of the American Ceramic Society 87 (2004) 47–54.
[27] H.R. Lashgari, A.R. Sufizadeh, M. Emamy, The effect of strontium on the microstructure and wear properties of A356–10%B_4C cast composites, Materials & Design 31 (2010) 2187–2195.
[28] F. Toptan, I. Kerti, L.A. Rocha, Reciprocal dry sliding wear behaviour of B_4C_p reinforced aluminium alloy matrix composites, Wear 290–291 (2012) 74–85.
[29] S. Wu, Y. You, P. An, T. Kanno, H. Nakae, Effect of modification and ceramic particles on solidification behavior of aluminum-matrix composites, Journal of Materials Science 37 (2002) 1855–1860.
[30] P. Rohatgi, R. Asthana, The solidification of metal-matrix particulate composites, JOM: The Journal of The Minerals Metals & Materials Society 43 (1991) 35–41.
[31] A. Patel, A. Bhabhor, V. Patel, A review on effect of grain refinement and modification on the dry sliding wear behaviour of eutectic Al–Si alloys, International Journal of Engineering Research and Applications (IJERA) 2 (2012) 2417–2421.
[32] J.M.G. De Salazar, A. Ureña, S. Manzanedo, M.I. Barrena, Corrosion behaviour of AA6061 and AA7075 reinforced with Al_2O_3 particles in aerated 3.5% chloride solutions: potentiodynamic measurements and microstructure evaluation, Corrosion Science 41 (1999) 529–545.
[33] A. Kennedy, B. Brampton, The reactive wetting and incorporation of B_4C particles into molten aluminium, Scripta Materialia 44 (2001) 1077–1082.
[34] O. Sarikaya, S. Anik, S. Aslanlar, S. Cem Okumus, E. Celik, Al–Si/B_4C composite coatings on Al–Si substrate by plasma spray technique, Materials & Design 28 (2007) 2443–2449.
[35] B.-S. Lee, S. Kang, Low-temperature processing of B_4C–Al composites via infiltration technique, Materials Chemistry and Physics 67 (2001) 249–255.
[36] F. Toptan, A. Kilicarslan, I. Kerti, The effect of Ti addition on the properties of Al–B_4C interface: a microstructural study, Materials Science Forum 636–637 (2010) 192–197.
[37] F. Toptan, A. Kilicarslan, A. Karaaslan, M. Cigdem, I. Kerti, Processing and microstructural characterisation of AA 1070 and AA 6063 matrix B_4C_p reinforced composites, Materials & Design 31 (2010) S87–S91.
[38] F. Toptan, I. Kerti, A. Sagin, M. Cigdem, S. Daglilar, F. Yuksel, Microstructural Properties and Wear Behaviour of $AlSi_9Mg$ matrix B_4C_p reinforced composites, in: TMS Annual Meeting 2, 2011: pp. 837–842.
[39] T.M. Yue, J.K. Yu, H.C. Man, Corrosion behavior of aluminum 2009/SiC composite machined to different conditions, Journal of Materials Science Letters 21 (2009) 1069–1072.
[40] A.J. Pyzik, D.R. Beaman, Al–B–C phase development and effects on mechanical properties of B_4C/Al-derived composites, Journal of American Ceramic Society 78 (1995) 305–312.
[41] G. Arslan, F. Kara, S. Turan, Quantitative X-ray diffraction analysis of reactive infiltrated boron carbide–aluminium composites, Journal of the European Ceramic Society 23 (2003) 1243–1255.
[42] N. Frage, L. Levin, N. Frumin, M. Gelbstein, M.P. Dariel, Manufacturing B_4C–(Al, Si) composite materials by metal alloy infiltration, Journal of Materials Processing Technology 143–144 (2003) 486–490.
[43] Z. Zhang, X.-G. Chen, A. Charette, Particle distribution and interfacial reactions of Al–7%Si–10%B_4C die casting composite, Journal of Materials Science 42 (2007) 7354–7362.
[44] Q. Feng, T. Li, H. Teng, X. Zhang, Y. Zhang, C. Liu, et al., Investigation on the corrosion and oxidation resistance of Ni–Al_2O_3 nano-composite coatings prepared by sediment co-deposition, Surface and Coatings Technology 202 (2008) 4137–4144.
[45] K.H. Seah, M. Krishna, V. Vijayalakshmi, J. Uchil, Corrosion behaviour of garnet particulate reinforced LM13 Al alloy MMCs, Corrosion Science 44 (2002) 917–925.
[46] I. Garcia, A. Conde, G. Langelaan, J. Fransaer, J.P. Celis, Improved corrosion resistance through microstructural modifications induced by codepositing SiC-particles with electrolytic nickel, Corrosion Science 45 (2003) 1173–1189.
[47] T. Lampke, A. Leopold, D. Dietrich, G. Alisch, B. Wielage, Correlation between structure and corrosion behaviour of nickel dispersion coatings containing ceramic particles of different sizes, Surface and Coatings Technology 201 (2006) 3510–3517.
[48] P.P. Trzaskoma, E. Mccafferty, C.R. Crowe, Corrosion behavior of SiC/Al metal matrix composites, Journal of the Electrochemical Society 130 (1983) 1804–1809.
[49] S. Mischler, S. Debaud, D. Landolt, Wear-accelerated corrosion of passive metals in tribocorrosion systems, Journal of The Electrochemical Society 145 (1998) 750–758.
[50] M.T. Mathew, E. Ariza, L.A. Rocha, A.C. Fernandes, F. Vaz, TiC_xO_y thin films for decorative applications: tribocorrosion mechanisms and synergism, Tribology International 41 (2008) 603–615.

[51] R. Ipek, Adhesive wear behaviour of B_4C and SiC reinforced 4147 Al matrix composites (Al/B_4C–Al/SiC), Journal of Materials Processing Technology 162–163 (2005) 71–75.
[52] D.P. Mondal, S. Das, High stress abrasive wear behaviour of aluminium hard particle composites: effect of experimental parameters, particle size and volume fraction, Tribology International 39 (2006) 470–478.
[53] C.S. Lee, Y.H. Kim, K.S. Han, Wear behaviour of aluminium matrix composite materials, Journal of Materials Science 27 (1992) 793–800.
[54] H. Ahlatci, T. Koçer, E. Candan, H. Çimenoğlu, Wear behaviour of Al/(Al_2O_{3p}+-SiC_p) hybrid composites, Tribology International 39 (2006) 213–220.
[55] R.N. Rao, S. Das, D.P. Mondal, G. Dixit, Effect of heat treatment on the sliding wear behaviour of aluminium alloy (Al–Zn–Mg) hard particle composite, Tribology International 43 (2010) 330–339.
[56] S.A. Alidokht, A. Abdollah-zadeh, S. Soleymani, T. Saeid, H. Assadi, Evaluation of microstructure and wear behavior of friction stir processed cast aluminum alloy, Materials Characterization 63 (2012) 90–97.
[57] K.G. Basavakumar, P.G. Mukunda, M. Chakraborty, Influence of grain refinement and modification on dry sliding wear behaviour of Al–7Si and Al–7Si–2.5Cu cast alloys, Journal of Materials Processing Technology 186 (2007) 236–245.
[58] T.M. Chandrashekharaiah, S.A. Kori, Effect of grain refinement and modification on the dry sliding wear behaviour of eutectic Al–Si alloys, Tribology International 42 (2009) 59–65.
[59] Y.B. Liu, J.D. Hu, Z.Y. Cao, P.K. Rohatgi, Wear resistance of laser processed Al–Si–graphitep composites, Wear 206 (1997) 83–86.
[60] A.L. Kearney, Properties of cast aluminum alloys, in: ASM Handbook, vol. 2, ASM International152–177.